Evolution of Hexagonal Patterns from Controlled Initial Conditions in a Bénard-Marangoni Convection Experiment

Denis Semwogerere and Michael F. Schatz*

Center for Nonlinear Science and School of Physics, Georgia Institute of Technology, Atlanta, Georgia 30332-0430

(Received 16 June 2001; revised manuscript received 10 October 2001; published 16 January 2002)

We report quantitative measurements of both wave number selection and defect motion in nonequilibrium hexagonal patterns. A novel optical technique ("thermal laser writing") is used to imprint initial patterns with selected characteristics in a Bénard-Marangoni convection experiment. Initial patterns of ideal hexagons are imposed to determine the band of stable pattern wave numbers while initial patterns containing an isolated penta-hepta defect are imprinted to study defect propagation directions and velocities. The experimental results are compared to recent theoretical predictions.

DOI: 10.1103/PhysRevLett.88.054501 PACS numbers: 47.54.+r, 47.20.−k, 61.72.Ji

A wide variety of nonequilibrium systems exhibit cellular patterns with hexagonal symmetry; examples include volcanic basalt columns [1], nanometer-scale anodization pores [2], along with other cases found in hydrodynamics, nonlinear optics, chemistry, and biology [1,3,4]. For a given system, the observed pattern is typically not unique but is one of many possible planforms, even when the system's external conditions are fixed. Competition can even arise between ideal patterns of 2D, perfect hexagons, where each planform possesses a different characteristic length scale. Defects are believed to play a central role in the process of pattern selection [4]. In hexagonal planforms, the most common defect is a penta-hepta defect (PHD), in which a pentagonal cell and a neighboring heptagonal cell are paired together and embedded in a lattice of otherwise hexagonal cells (Fig. 1). Recent theoretical [5,6] and experimental [7] investigations have studied the dynamics of PHDs; nevertheless, the mechanisms by which defects lead to the selection of nonequilibrium cellular patterns are still poorly understood.

In this paper, we report on experiments of Bénard-Marangoni convection where three fundamental behaviors of nonequilibrium hexagonal patterns have been measured. Hexagons arise at the onset of convection and are stable for a range of wave numbers limited by secondary instabilities. Imposing perfect hexagonal patterns as initial conditions enables the first measurement of the stable wave number band for hexagons (Fig. 2). This wave number band is related to the dynamics of PHDs, which are studied by imposing a single defect embedded in a hexagonal pattern. In particular, the defect typically moves in a way that selects a wave number near the center of the stable band (Figs. 3 and 4). Our studies demonstrate, for the first time, that the average direction of the defect motion depends strongly on the wave numbers in accord with recent theoretical predictions [6] (Fig. 3). Studies of the defect motion also reveal time-dependent behavior not described by current models of PHD motion (Figs. 3 and 5). This time dependence is related to elementary topological processes observed in a wide variety of cellular patterns [1].

The experiments are typically performed on a silicone oil layer of depth 0.094 ± 0.003 cm and viscosity 10 cS that is bounded from below by a 1-cm-thick aluminum mirror. A 5-mm-thick zinc sulfide window lies above the liquid layer, separated from the liquid layer by a uniform air layer of depth 0.074 ± 0.003 cm. The liquid is confined by a Teflon-coated aluminum sidewall ring of inner diameter 7.62 ± 0.001 cm, yielding radius to height ratio 40.5 of the convecting region. The liquid and the air layer depths each vary by less than 0.1% over the central 75% of the convecting region, as measured interferometrically. The window is maintained at $22.39 \pm 0.03\,^{\circ}\mathrm{C}$ by closed-loop circulation of temperature-controlled carbon disulfide in contact with the window. The use of zinc sulfide windows and carbon disulfide cooling permits optical access to the experiment at wavelengths in both the visible spectrum for visualizing the flow and the infrared spectrum for perturbing the flow with a laser. A temperature gradient is imposed across the liquid layer by heating the mirror under computer control. When the imposed temperature difference across the liquid layer ΔT is sufficiently small, the surface tension $\sigma(T)$ at the liquid-gas interface is uniform; however, when ΔT exceeds $1.57 \pm 0.01\,^{\circ}\mathrm{C}$, instability causes temperature-induced surface tension variations (thermocapillarity) that drive cellular flow patterns in the bulk (Fig. 1). Thermocapillarity dominates over buoyancy, which is also present for heating from below, since the quantity $\Gamma = \frac{\sigma_T}{\rho \alpha g d^2} > 1$ ($\Gamma \approx 8.5$, typically), where ρ is the liquid's density, α is the thermal expansivity, $\sigma_T \equiv -\frac{d\sigma}{dT}$ is the surface tension temperature coefficient, and g is the gravitational acceleration [8]. The time scale in the experiment is set by the vertical diffusion time, $\tau_v = d^2/\kappa = 8.8$ s, where κ is the liquid's thermal diffusivity.

The shadowgraph technique [9] is used to visualize patterns. Images are digitized and a reference background image is subtracted from each data image to improve the signal-to-noise ratio. The patterns are analyzed using a variety of Fourier and complex demodulation techniques to extract the spatial dependence of the pattern wave number, amplitude, and phase [7,10,11].

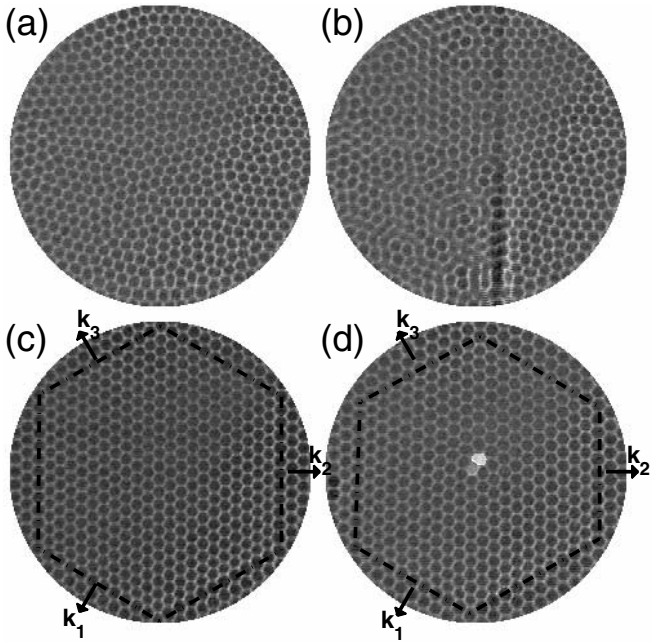

FIG. 1. The process of imposing patterns in Bénard-Marangoni convection is shown for $\epsilon = 0.28$ using shadowgraphy of the liquid layer's planform. Warm liquid upwells in the cell centers (dark areas) and flows down at the cell edges (bright lines). (a) Disordered patterns form when the temperature difference across a liquid layer is increased rapidly above convective onset. (b) An infrared laser is rapidly scanned across the free surface of the layer; the beam's position is indicated by the dark vertical line in the center of the pattern. This selective heating forces the flow to rearrange into a desired planform, either (c) ideal hexagons or (d) an isolated penta-hepta defect surrounded by hexagonal cells. In both cases, the patterns may be described by the superposition of three plane waves (rolls) with wave vectors $\mathbf{k}_1$, $\mathbf{k}_2$, and $\mathbf{k}_3$ mutually separated by 120°. Outside the dot-dashed lines in (c) and (d) laser heating is continually applied to decouple the dynamics of the planform interior from that near the sidewall.

Patterns are imposed using an infrared CO_2 laser scanner ("thermal laser printer") that radiatively heats the liquid-air interface (Fig. 1). Thermal imprinting with high intensity lamps was used by others to study wave number selection in Rayleigh-Bénard convection [12]. In our case, imprinting occurs when an infrared laser beam strikes the liquid layer. The infrared radiation is strongly absorbed by the liquid, creating a local hot spot near the liquid-air interface. The surface tension at the hot spot is reduced since $\frac{d\sigma}{dT} < 0$. Liquid is pulled away from the hot spot toward cooler regions at the interface and is replaced by fluid flowing up from the layer below. Thus, laser-induced hot spots determine areas of upflow in the convection pattern. By scanning the laser across the layer, a hexagonal array of upflows can be imposed. This method can even alter a preexisting convection pattern when the laser power is sufficiently large. The imposed pattern is typically established in 30 s, whereupon the laser heating is turned off in the central 75% of the convecting layer and the subsequent evolution of the pattern is studied. Laser heating

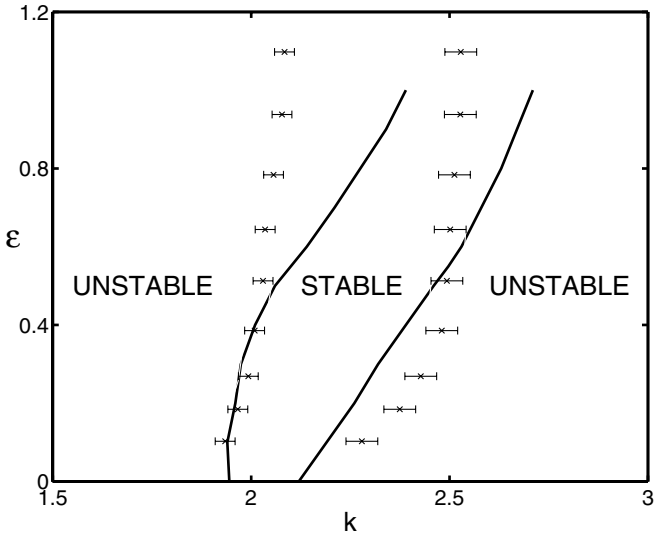

FIG. 2. The band of stable wave numbers k for ideal hexagonal patterns ($k = k_1 = k_2 = k_3$) is shown for a range of reduced temperatures ϵ. The experimentally determined stable wave numbers lie between the low and high k boundaries ($\times$) and are compared with the theoretical predictions (solid lines) of Bestehorn [14].

is maintained in the outer 25% of the convecting layer to decouple the pattern dynamics in the interior of the apparatus from flows driven by temperature nonuniformities at the sidewall. Typically, the wave number imposed near the sidewall is identical to that imposed in the interior; if there are significant mismatches in the imposed wave numbers between the interior region and the sidewall region, then defects often form at the boundary and propagate into the pattern interior, leading to inconsistent measurements.

The range of stable wave numbers (Fig. 2) is measured by observing the time evolution of initially perfect hexagons with wave number $k = |\mathbf{k}_1| = |\mathbf{k}_2| = |\mathbf{k}_3|$. These measurements are inspired by the classic experimental studies [12] of the stability of single plane waves (rolls) in pure buoyancy-driven (Rayleigh-Bénard) convection,

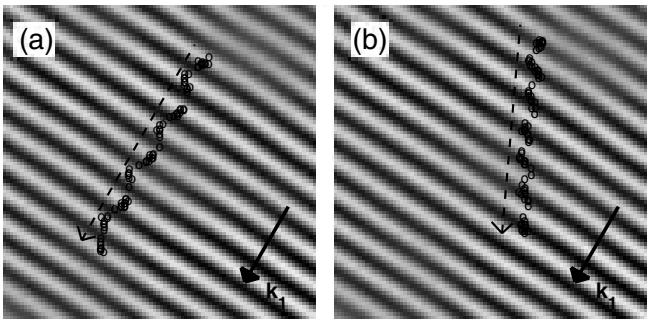

FIG. 3. Trajectory of an isolated penta-hepta defect for equal (a) and unequal (b) wave numbers for $\epsilon = 0.28$. Dashed arrows indicate direction of defect motion. The trajectories are plotted on the defect-free mode $\mathbf{k}_1$. (a) For ($k_1 = k_2 = k_3 = 2.37$) path is roughly parallel to $\mathbf{k}_1$. (b) Trajectory after k_2 is decreased by less than 5% to 2.31.

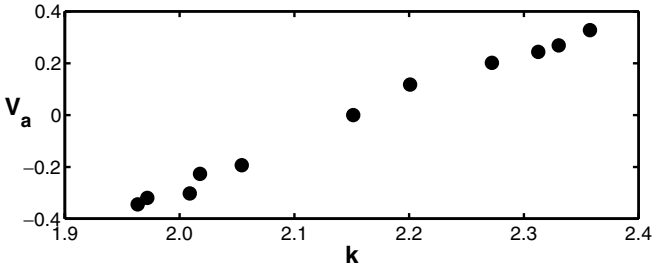

FIG. 4. Average defect velocity along $\mathbf{k}_1$ is plotted as a function of wave number k for $k_1 = k_2 = k_3$ with $\epsilon = 0.28$. Defect velocity parallel to $\mathbf{k}_1$ is positive, antiparallel to $\mathbf{k}_1$ is negative.

where well-known theoretical predictions (the "Busse balloon") have identified secondary instabilities limiting the stable wave numbers for rolls [13]. More recently, theoretical predictions of secondary instabilities for Bénard-Marangoni convection have been made by Bestehorn [14]. Ideal hexagonal patterns within the experimental band are observed to be time independent for the entire duration of a given experiment ($\lesssim 10^4 \tau_v$). However, outside the band ideal hexagons are unstable; point defects (typically PHDs) form either at the lateral boundary or in the bulk and propagate rapidly throughout the pattern inducing disorder. This motion of defects is transient, the dynamics are relaxational, and the pattern eventually ($\approx 300\ \tau_v$) reorders itself and settles down into a time-independent state of non-ideal hexagons, i.e., $k_1 \neq k_2 \neq k_3$ (rhombs [15]), with a mean wave number that always lies within the range of stable wave numbers for ideal hexagonal patterns (Fig. 2).

The agreement between experiment and theory [14] for the stability boundaries is better for smaller ϵ than for larger ϵ (Fig. 2). For $\epsilon \lesssim 0.5$, experiment and theory agree quantitatively for the low k boundary of the stable band, which exhibits little change as ϵ increases. At the high k boundary for $\epsilon \lesssim 0.5$, both experiment and theory exhibit a shift toward larger k with increasing ϵ; however, the experimentally determined high k boundary typically lies outside that predicted by theory. By contrast, for $\epsilon \gtrsim 0.5$, the theoretically predicted boundaries for both low and high k shift toward larger values of k with increasing ϵ while the experimentally determined boundaries exhibit little dependence on ϵ. The discrepancies between theory and experiment may be due to differences between the conditions of the experiments ($\Gamma \approx 8.5$ at a Prandtl number of 100) and of the theory ($\Gamma \approx 2.7$ at infinite Prandtl number) [14].

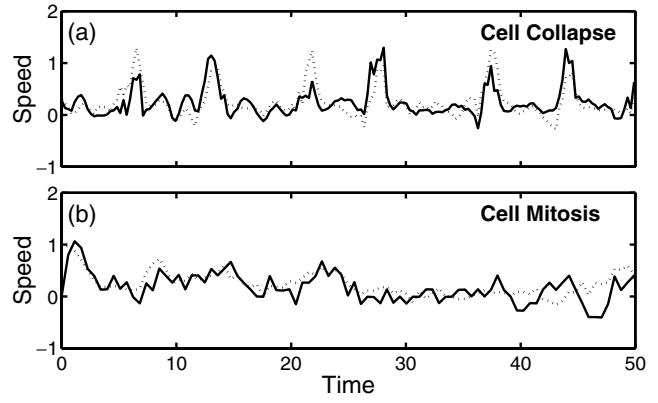

FIG. 5. Time series of defect speeds for $k_1 = k_2 = k_3$ at $\epsilon = 0.28$ corresponding to (a) pentagonal cell collapse with $k = 2.23$ and (b) heptagon mitosis with $k = 1.95$. The solid line indicates the magnitude of velocity perpendicular to $\mathbf{k}_2$, while the dashed line shows the magnitude of velocity perpendicular to $\mathbf{k}_3$. Pentagonal cell collapse is characterized by jumps in PHD motion that occur alternately between directions perpendicular to $\mathbf{k}_2$ and perpendicular to $\mathbf{k}_3$; this alternating character is shown in (a). By contrast, PHD motion during heptagon mitosis is smoother, as shown in (b).

Our findings differ qualitatively from those of Cerisier *et al.,* who observed that ideal hexagons, imposed using a mechanical method, slowly evolve to disordered patterns with a unique average wave number [16]. In our experiments, a narrow range of stable average wave numbers is observed when no lateral boundary is imposed; in this case, the creation and annihilation of defects confined to the lateral boundaries stretches or shrinks k_1, k_2, k_3 of initially ideal hexagons, leading to the formation of rhombs.

The dynamics of PHDs are studied by observing the time evolution of a single PHD initially embedded in the center of a hexagonal pattern (Fig. 1d). This pattern can also be described as a superposition of three rolls with well-defined k_1, k_2, k_3 far from the defect. One of the rolls is defect-free ($\mathbf{k}_1$ in Fig. 1d) and the other two rolls ($\mathbf{k}_2, \mathbf{k}_3$ in Fig. 1d) each contain a single dislocation located at the PHD core. For any counterclockwise closed path encircling the defect core, phase jumps of -2π for $\mathbf{k}_2$ and $+2\pi$ for $\mathbf{k}_3$ are found; in other words, the dislocations have opposite phase winding numbers [10]. The position of the PHD is determined by using complex demodulation to find the location of the phase singularity in $\mathbf{k}_3$ rolls. (Use of the $\mathbf{k}_2$ dislocation yields similar results.)

The mean propagation direction of a single PHD depends strongly on the relative magnitudes k_2 and k_3 in accord with theoretical predictions [6]. When patterns are imposed with $k_1 = k_2 = k_3$ at the lateral boundary, the defect propagates parallel or antiparallel to $\mathbf{k}_1$ (Fig. 3a). This direction is unchanged, even when k_1 is varied to differ from k_2, k_3. However, when k_2 and k_3 differ, the mean propagation direction changes and depends on the ratio $\frac{k_2}{k_3}$ (Fig. 3b). It is worth noting that in experiments on an *equilibrium* system (a planar array of soap bubbles) with $k_1 = k_2 = k_3$, PHDs are found to propagate *perpendicular* to $\mathbf{k}_1$ [7].

For $k_1 = k_2 = k_3$, the choice between parallel vs antiparallel propagation along $\mathbf{k}_1$ is related to the band of stable wave numbers for ideal hexagonal patterns (Figs. 2 and 4). Simply put, the defect moves in a direction that adjusts the local wave number *near the defect* to a value that is closer to the center of the stable wave number band

(Fig. 2). For wave numbers at large (small) k, defect propagation parallel (antiparallel) to $\mathbf{k}_1$ removes (adds) two rows of hexagonal cells; the dislocations of the rolls $\mathbf{k}_2, \mathbf{k}_3$ move by a combination of climb and glide to eliminate (add) a roll for each plane wave. There is a value of wave number where the defect is stationary (Fig. 4). These observations are in qualitative agreement with predictions from amplitude equations [6]. However, the models predict defect velocities go to zero for $k = k_c$, the critical wave number at onset from linear stability theory. We find that the value of k for stationary PHDs differs from k_c for finite values of ϵ.

A closer examination of the defect motion shows that it is time dependent, a feature that is not captured by current theoretical models which take as an ansatz that the velocity is steady. When the defect propagates parallel to $\mathbf{k}_1$ ($\mathbf{v}_a > 0$ in Fig. 4) it does so by alternately eliminating a cell from rows perpendicular to the $\mathbf{k}_2$ and $\mathbf{k}_3$ directions. The resulting path is spatially nonuniform, but the overall direction is parallel to $\mathbf{k}_1$ (Fig. 3a). Time dependence is due primarily to collapse of pentagonal cells, which occurs through combinations of elementary topological T1 and T2 processes [1]. The T1 processes cause slow rearrangement of the cell downflow intersections, resulting in small defect speeds. Intermittently, however, T1 and T2 processes together cause pentagons to vanish, resulting in a large jump in speed (Fig. 5a). In terms of the underlying roll patterns the jumps in speed correspond to glide of dislocations occurring alternately in the $\mathbf{k}_2$ and the $\mathbf{k}_3$ modes. This speed jump also corresponds to displacement of the defect by approximately π/k parallel to $\mathbf{k}_1$.

When the defect trajectory is antiparallel to $\mathbf{k}_1$, the defect speed is time dependent with smoother variations (Fig. 5b). In this case the motion is a result of the *creation* of cells by the qualitatively different topological process of cell division (mitosis) of heptagonal cells [1]. Heptagon mitosis results in displacement of the defect by approximately π/k antiparallel to $\mathbf{k}_1$.

In summary, our results demonstrate that the use of controlled initial conditions in experiments permits measurements of the dynamics of nonequilibrium patterns, both with and without defects. Work is currently in progress to explore the band of stable wave numbers for nonideal hexagonal patterns for a wide range of ϵ. Work is also underway to explore the use of multipoint heating as feedback for controlling patterns; in particular, we are exploring methods of dynamically altering the trajectories of defects in hexagonal patterns.

We thank Guenter Ahlers, Kapil Bajaj, Nathan Currier, and William Ogle for the use of their computer codes for local wave number analysis of patterns. We also thank Lev Tsimring for reading an early version of the paper and for helpful comments. Support for this work by the National Science Foundation (CTS-9876590) and the Research Corporation (CS0657) is gratefully acknowledged.

*Electronic address: mike.schatz@physics.gatech.edu

[1] D. Weaire and N. Rivier, Contemp. Phys. **25**, 59 (1984).
[2] L. Zhang, H. S. Cho, F. Li, R. M. Metzger, and W. D. Doyle, J. Mater. Sci. Lett. **17**, 291 (1998).
[3] W. J. Firth, Proc. SPIE Int. Soc. Opt. Eng. (U.S.A.) **2039**, 290 (1993).
[4] M. C. Cross and P. C. Hohenberg, Rev. Mod. Phys. **65**, 851 (1993).
[5] M. I. Rabinovich and L. S. Tsimring, Phys. Rev. E **49**, R35 (1994).
[6] L. S. Tsimring, Phys. Rev. Lett. **74**, 4201 (1995); Physica (Amsterdam) **89D**, 368 (1996).
[7] T. Tam, D. Ohata, and M. Wu, Phys. Rev. E **61**, R9 (2000).
[8] M. F. Schatz and G. P. Neitzel, Annu. Rev. Fluid Mech. **33**, 93 (2001).
[9] J. R. de Bruyn, E. Bodenschatz, S. W. Morris, S. P. Trainoff, Y. Hu, D. S. Cannell, and G. Ahlers, Rev. Sci. Instrum. **67**, 2043 (1996).
[10] S. Ciliberto, P. Coullet, J. Lega, E. Pampaloni, and C. Pérez-García, Phys. Rev. Lett. **65**, 2370 (1990).
[11] D. A. Egolf, I. V. Melnikov, and E. Bodenschatz, Phys. Rev. Lett. **80**, 3228 (1998).
[12] M. M. Chen and J. A. Whitehead, J. Fluid Mech. **31**, 1 (1968); F. H. Busse and J. A. Whitehead, J. Fluid Mech. **47**, 305 (1971).
[13] F. H. Busse, J. Math. Phys. **46**, 140 (1967).
[14] M. Bestehorn, Phys. Rev. E **48**, 3622 (1993).
[15] Q. Ouyang, G. H. Gunaratne, and H. L. Swinney, Chaos **3**, 707 (1993).
[16] P. Cerisier, C. Pérez-García, and R. Occelli, Phys. Rev. E **47**, 3316 (1993).